Single-platelet nanomechanics measured by high-throughput cytometry

Resolving the nanomechanics of platelet contraction, the driver of blood clot stiffening, towards clinical translation

David R. Myers[1,2,3,4,5], Yongzhi Qiu[1,2,3,4,5], Meredith E. Fay[1,2,3,4,5], Michael Tennenbaum[6], Daniel Chester[7,8], Jonas Cuadrado[6], Yumiko Sakurai[1,2,3,4,5], Jong Baek[1,2,3,4,5], Reginald Tran[1,2,3,4,5], Jordan Ciciliano[1,2,3,4,5], Byungwook Ahn[1,2,3,4,5], Robert Mannino[1,2,3,4,5], Silvia Bunting[9], Carolyn Bennett[1], Michael Briones[1], Alberto Fernandez-Nieves[6], Michael L. Smith[10], Ashley Carson Brown[7,8], Todd Sulchek[11], Wilbur A. Lam[1,2,3,4,5]

[1] Department of Pediatrics, Division of Pediatric Hematology/Oncology, Aflac Cancer Center and Blood Disorders Service of Children's Healthcare of Atlanta, Emory University School of Medicine, Atlanta, GA 30322

[2] The Wallace H. Coulter Department of Biomedical Engineering, Georgia Institute of Technology & Emory University, Atlanta, GA, 30332

[3] Winship Cancer Institute of Emory University, Atlanta, GA, 30322

[4] Parker H. Petit Institute of Bioengineering and Bioscience, Georgia Institute of Technology, Atlanta, GA 30332

[5] Institute for Electronics and Nanotechnology, Georgia Institute of Technology, Atlanta, GA 30332

[6] School of Physics, Georgia Institute of Technology, Atlanta, GA, 30332

[7] Department of Biomedical Engineering, North Carolina State University and University of North Carolina Chapel Hill, Raleigh, NC 27695

[8] Comparative Medicine Institute at North Carolina State University, Raleigh, NC 27695

[9] Department of Pathology, Emory University School of Medicine, Atlanta, GA 30322

[10] Department of Biomedical Engineering, Boston University, Boston, MA, 02215

[11] George W. Woodruff School of Mechanical Engineering, Georgia Institute of Technology, Atlanta, GA, 30332

Corresponding Author:

Wilbur A. Lam
Address: 2015 Uppergate Dr, NE; Emory Children's Center - Room 448; Atlanta, GA 30322
Email: wilbur.lam@emory.edu
Phone: 404-727-7473
Fax: 404-727-4455

Hemostasis occurs at sites of vascular injury where flowing blood forms a clot, a dynamic and heterogenous fibrin-based biomaterial. Paramount in the clot's capability to stem hemorrhage are its changing mechanical properties, the major driver of which are the contractile forces exerted by platelets against the fibrin scaffold [1]. However, how platelets transduce microenvironmental cues to mediate contraction and alter clot mechanics is unknown yet clinically relevant, as overly softened and stiffened clots are associated with bleeding [2] and thrombotic disorders [3], respectively. To that end, we developed a high-throughput platelet contraction cytometer to quantify single platelet contraction forces in different clot microenvironments and found that platelets, via the Rho/ROCK pathway, synergistically couple mechanical and biochemical inputs to mediate contraction. Moreover, highly contractile platelet subpopulations present in healthy controls are conspicuously absent in a subset of patients with undiagnosed bleeding diatheses and therefore may function as a clinical diagnostic biophysical biomarker.

During clot formation, various physiological cues such as damaged blood vessels or shear forces initiate platelet activation, adhesion, and the coagulation cascade, which lead to fibrin polymerization. Activated platelets then aggregate and bind to the nascent fibrin network via the $\alpha_{IIb}\beta_3$ integrin and undergo actomyosin-mediated muscle-like contraction (Extended Data Figure 1, Extended Data Video 1), which significantly decreases the overall clot size while increasing clot stiffness by several orders of magnitude. While this platelet-driven clot contraction has been well described in the literature, the mechanistic underpinnings and especially the biochemical and biophysical parameters that mediate this process remain poorly understood due to technological barriers. Current assays provide force measurements during clot contraction,

establishing changes in average platelet force with different diseases [4], but these operate at the bulk level [1,3,5,6].

As recent studies demonstrate, microenvironmental cues such as mechanical properties of the underlying matrix substrate [7,8], matrix geometry [9], biochemical conditions [10], and shear stress [11,12] all mediate platelet physiology at the single cell level. In addition, clots in the dynamic hemodynamic environment are innately heterogeneous in which shear rate, fibrin architecture, and agonist concentration all vary significantly throughout the same clot. Therefore, a high-throughput, single platelet contraction assay is needed to establish and understand the "fundamental driver" of clot contraction, that is, how an individual platelet integrates biochemical and biophysical inputs to contract against the microenvironmental fibrin/ogen network. As fibrin mechanics have been well characterized, [13] deciphering this fundamental driver of clot contraction is the "missing link" needed to reconstruct higher order clot behavior and to obtain a comprehensive physical understanding of clot mechanics at multiple length scales.

To that end, we developed a microfabricated chip that simultaneously measures the contractile force of hundreds of individual platelets adherent on substrates with varied mechanical stiffnesses spanning the physiological range, while controlling the biochemical and shear microenvironment. This system overcomes technical barriers associated with existing techniques used for single cell analysis, such as the low throughput of atomic force microscopy [8]; the high computational needs of traction force microscopy [14]; or aggregate platelet measurements with micropillar arrays [15]. Here, an activated platelet adheres to and spans a fibrinogen microdot pair and contracts the microdot pair together (Figure 1a-c, Extended Data Video 4). As contraction force is proportional to the fibrinogen microdot area and microdot displacement, relatively high-

throughput measurements conducted with single cell resolution (Figure 1d-e), effectively creating a "platelet contraction cytometer." Imaging studies of the fibrin architecture in a developing clot informed microdot spacing/size (Extended Data Figure 1, Supplementary Information, and Methods: Optimizing plating), recapitulating the geometry of the *in vivo* platelet microenvironment. Since the platelet behavior of spanning and pulling microdots together is morphologically similar to clot behavior of platelets in fibrin meshes, trends observed in this system are expected to match those observed in a 3D system. Hydrogel stiffnesses of 5 – 100 kPa were used to approximate the range of mechanical environments encountered by a platelet within a clot (Extended Data Figure 2).

Because local biochemical agonists, hemodynamics, and mechanical properties of the clot directly mediate platelet physiology, we further refined our microfluidic system to enable encapsulation of micropatterned hydrogels of different stiffnesses in adjacent microchannels, enabling simultaneous testing of substrate stiffnesses, shear conditions, or agonist concentrations (Figure 2a-b, Extended Data Figure 3). Each measurement of contraction force is not influenced by confounding effects such as the underlying substrate or neighboring platelet contraction, as shown by measurements of the gel thickness, stiffness, and microdot independence (Extended Data Figure 4). As thrombin, a potent physiologic platelet activator, and substrate stiffness both mediate different signaling pathways [7] that converge in clot contraction [16], the contraction cytometer was used to quantify how platelets synergistically integrate both biochemical and microenvironmental mechanical inputs to modulate contractile forces. Thrombin also converts fibrinogen to monomeric fibrin, enabling the experiments to more closely resemble the *in vivo* clotting environment [17,18].

Platelets have a highly nonlinear force curve (Figure 3) with maximum "peak" contraction force at moderate substrate stiffness and thrombin concentration, both within the physiologic range found in clots. While the observation of a peak force is similar to myocytes [19], platelets are unique in that output force is both mediated and requires a biochemical and mechanical input. Surprisingly, platelet contraction force is independent of shear stress (Extended Data Figure 5). As measurements are obtained after initial adhesion in our protocol, this independence suggests that shear effects are most significant in the early phases of activation. Interestingly, at the highest tested thrombin concentrations (5U/mL) characteristic of prothrombotic conditions, the subset of low contractile force platelets increases, thereby lowering the average platelet force (Figure 3). In addition, at highest stiffness conditions, platelets contract at lower forces demonstrating that this phenomenon is not simply due to the sensitivity limit of our system (Extended Data Figure 6).

Mechanistically, we discovered that the substrate stiffness-mediated platelet contractile force is highly dependent on the Rho/ROCK pathway (Figure 4a). To elucidate the underlying mechanotransductive mechanisms of how clot stiffness mediates contraction force, we employed two pharmacologic inhibitors of myosin light chain phosphorylation, ML7 and Y276232, which inhibit Ca^{2+}/calmodulin-dependent myosin light chain kinase (MLCK) and Rho kinase (ROCK), respectively. In light of previous results showing that MLCK and not ROCK is essential to mechanosensitive spreading [7], our results showing ROCK and not MLCK is essential to mechanosensitive contraction highlight that the MLCK and ROCK pathways serve complementary mechanosensing functions in platelets. Previous studies have shown that the Rho/ROCK pathway is upregulated in cells adhered onto stiff environments [20] (RhoA) and is associated with stress fiber formation [21] (ROCK). Consistent with this idea is the observation

121 that actin polymerization weakly correlates with increasing platelet contractile force (Extended
122 Data Figure 7). As the platelet is anucleate, our data also demonstrate that mechanosensitive
123 contraction can occur in the absence of gene expression.

124 To determine whether these findings on single platelets are related to changes in the bulk
125 material properties of a blood clot, we conducted ROCK-inhibition experiments using standard
126 bulk clot contraction assays and bulk clot rheometry. We observed that ROCK-inhibition impairs
127 bulk clot contraction as compared to the untreated control clots (Figure 4b), whereas MLCK
128 inhibition did not alter clot contraction (Figure 4c). Bulk clot rheometry experiments, which
129 enabled simultaneous measurements of storage and loss moduli as well as bulk tensile forces,
130 revealed that while both control and ROCK-inhibited clots undergo a dramatic stiffening process
131 during the course of the experiment (Figure 4d), the exerted tensile forces differed but only at
132 later time points. Specifically, control and ROCK-inhibited clots apply similar forces during the
133 beginning of clot formation (Figure 4e) when the measured storage and loss moduli are low
134 (Figure 4d). Over time, as the clots stiffen (Figure 4d), ROCK-inhibited bulk clots begin to exert
135 lower tensile forces (Figure 4e) and plateau while the control continues to increase over time.
136 Taken together, these bulk clot contraction observations are consistent with our data on
137 individual platelet contractile force. In soft environments, both ROCK-inhibited individual
138 platelet forces and ROCK-inhibited bulk contraction forces are similar to matching controls in
139 bulk and at the single platelet level. In stiff environments, however, both ROCK-inhibited
140 individual platelet forces and ROCK-inhibited bulk contraction and forces are substantially
141 lower than matching controls. As changes in bulk contraction can be due to multiple reasons,
142 including changes in fibrin or rates of platelet contraction, our ROCK-inhibition single platelet
143 contraction data coupled with the bulk data, taken together, suggest that platelet contractile force

alone can mediate these changes in bulk material behavior of clots. Hence, our data on individual platelet behavior in varying microenvrionements is not only associated with bulk clot contraction but can even inform the mechanisms occurring in bulk. Interestingly, the storage and loss modulus are the same for both ROCK-inhibited and control (Figure 4d), which may be due to the fact that the storage modulus of a clot is a function of both the density of cross-linking points [22], as well as tensioning of loose fibrin fibers [23].

Since *in vitro* clot contraction impairment is associated with limiting the maximum force exerted by a platelet, we hypothesized that low contractile forces measured at the single platelet level are associated clinical bleeding disorders. To that end, we first measured the platelets from patients with impaired cytoskeletal machinery, which were expected to have lower contractile forces. Compared to healthy controls, patients with defective actomyosin machinery such as those with Wiskott Aldrich (WAS) syndrome, which involve mutations of the actin-related WAS protein gene, or MYH9-related disorders (MYH9RD), which involve mutations of the non-muscle myosin IIA gene, lack highly contractile platelets. Blood from WAS and MYH9 patients exhibit impaired bulk clot retraction, [24,25] but these studies could not definitively pinpoint specific dysfunction in platelet contraction [25]. In our system, platelets from these patients exhibited significantly lower contraction force compared to those from healthy individuals in both stiff (Figure 5a) and soft mechanical environments (Extended Data Figure 8). More specifically, in these patients, a larger platelet subpopulation exerts near zero contractile force on stiff environments than for healthy subjects - approximately 30% versus 6% of platelets. Our single platelet measurements suggest that in these disorders, the impaired clot retraction may be due to the inability of individual platelets to apply appropriate forces.

Diminished platelet contractile forces were also found in a subset of a small cohort of patients presenting with chronic bleeding symptoms but normal clinical hemostasis tests. Specifically, these individuals have either normal or low-normal laboratory values for complete blood count, coagulation screening tests, platelet function (via PFA-100 or platelet aggregometry), or von Willebrand disease panels (Extended Data Table 1, Extended Data Table 2). Interestingly, three of the five patients showed impaired platelet contractility on stiff gels (Figure 5a), with a notable platelet subpopulation with forces below 20nN. Our platelet contraction cytometer's capability to detect these previous undiagnosable patients with bleeding diatheses, independent of existing clinical tests of hemostasis, establishes it as a potential new category of diagnostic to evaluate for platelet dysfunction.

As shown above, a key capability of platelet contraction cytometry is single cell resolution and the detection of different platelet subpopulations based on contractility, providing a more nuanced understanding of what influences clot stiffening. Currently used contraction assays measure only bulk platelet contractility and do not detect the low contractile subpopulation that potentially correlates with disease. Even amongst our healthy donors, average platelet contractile forces varied considerably. However, platelet contractility cytometry revealed subpopulations of highly contractile platelets (with peaks at 30 nN and higher), which is consistent amongst all healthy donors (Figure 5b). We also observed individuals both with highly variable and highly consistent platelet contraction at different points in time (Extended Data Figure 9), indicating that platelet contraction force might be affected by a number of different physiological conditions, but in aggregate, establish a range that is consistently higher than the subset of bleeding patients described above. Our test then represents an important step towards the goal of personalized medicine.

By precisely controlling the mechanical, chemical, and shear microenvironments, this work defines the fundamental driver of clot stiffening, thereby providing important, clinically relevant insights into clot mechanics. The platelet contractility cytometer presented herein entails a simple fabrication process and represents a key technological advance in rapid, high-throughput, single cell force analysis. Models linking microscale measurements to macroscale clot mechanics are now possible, where they were previously hindered by the inherent mechanical complexity of fibrin and the lack of data on how single platelets sense their microenvironment and apply force. Our data shows for the first time that trends observed in individually contracting platelets are mirrored by changes in the bulk material properties of clots. Moreover, single platelet contraction measurements inform how the material properties of a nascent clot directly affect platelet contraction and vice-versa, a correlation not accomplished by bulk assays. Our data further suggests that platelet contraction cytometry has the potential to serve as a useful addition to existing clinical tests of platelet function, as platelet contraction does not correlate with the currently used biomarkers of platelet activation (Extended Data Figure 7). Our newfound understanding of how platelet actuation directly affects clot formation and mechanics can be used to guide diagnostic strategies for thrombosis and bleeding disorders. Similarly, our contraction data and findings of the involved mechanotransductive pathways (Rho/ROCK) inform the development of pharmacological agents aimed at optimizing clot stiffness. Finally, this reductionist assay could be used to provide insight into other physiologically common cell and fibrous matrix systems that are often used in tissue engineering [26].

Methods:

Device design: Fabrication

The device relies on the use of commercially available materials such as thin rolls of PDMS and rapid fabrication techniques such as laser cutting to achieve fabrication times of less than 8 hours per batch of devices (Extended Data Figure 3).

Laser cut gel mold

The first layer of the device will hold the polymerized patterned polyacrylamide gels and serve as the base layer. A laser cutter (Universal Laser Systems, VLS 3.5) is used to pattern long rectangular holes (1 mm x 25 mm) into a pre-fabricated sheet of PDMS (Rogers HT6240-0.01") (Extended Data Figure 3a). The PDMS sheets are ultrasonically cleaned with successive solutions of diluted Alconox, DI water, and ethanol. The sheets along with 24x40 mm No. 1 coverslips (Fisher Scientific) are then treated with an O_2 plasma (Harrick Plasma, PDC-32G) and covalently bonded together. The bonding is greatly improved after an overnight heat treatment at 60 C.

Once bonded together, the combined PDMS and coverslip piece was silanized. After an O_2 plasma treatment, pieces were incubated in a 10% (3-Aminopropyl)trimethoxysilane (Sigma 281778) /90% Ethanol/ 0.01% Glacial acetic acid solution for 90 min at 60C. The pieces were then vigorously rinsed with 70%ETOH/30% DI water three times, then rinsed with DI water three times. To improve the PDMS flexibility and surface properties, the pieces were left in DI water for 1 hour at room temperature. The pieces were then incubated with a 2% glutaraldehyde

231 solution at room temperature for 30 minutes, then rinsed with DI water, and dried with
232 compressed nitrogen.

233 **Ligand (fibrinogen) stamped coverslips and optimal concentration**

234 Stamped coverslips (No 1.5, 18mm x 18mm) were prepared using the lift-off method as
235 described previously [27] (Extended Data Figure 3b). The silicon mold to create the fibrinogen
236 microdots was etched using standard lithography and etching techniques to a depth of 800 nm.
237 Fibrinogen conjugated to AlexaFluor 488, 594, or 647 (Thermo Fisher Scientific) was used
238 depending on other selected fluorophores in the experiment. The fibrinogen was incubated
239 on10 mm x 10 mm x 3 mm PDMS squares at 30 μg/mL for 1 hour, rinsed off, and dried with
240 compressed nitrogen. The PDMS squares with incubated fibrinogen were then brought in contact
241 with O_2 treated silicon molds and removed to create a fibrinogen microdot pattern on the PDMS.
242 The microdot pattern was then transferred onto an O_2 plasma treated 18 mm x 18 mm coverslip.

243 Previous work has demonstrated that platelet spreading is greatly affected by the ligand density [28]
244 . Surprisingly, platelet spreading is enhanced on low ligand density surfaces as compared with
245 high ligand density surfaces. We attempted to both lower and increase the ligand density on our
246 gels approximately 10 fold by changing the concentration of fibrinogen incubated on the PDMS
247 stamps. For cases of low fibrinogen concentration on polyacrylamide gels, platelet adhesion was
248 greatly diminished on the patterned surface, precluding contraction measurements. In cases of
249 high fibrinogen concentration, the micropattern shape was often greatly deformed and of
250 inconsistent brightness upon hydrogel polymerization. As such, our tests focused on
251 concentrations of 30 μg/mL.

Polyacrylamide gel casting

To create wells for the polyacrylamide gel, the fibrinogen patterned coverslip was inverted and aligned over the hybrid 25 x 40 mm PDMS glass coverslip. This assembled piece was placed in an argon filled glovebox (MBraun UNIlab plus) after observing a 30 minute incubation under vacuum in the glovebox antechamber. In the glovebox, and directly prior to use, pre-mixed polyacrylamide solutions with appropriate ratios of acrylamide to bis-acrylamide in PBS, were mixed with N,N,N′,N′-Tetramethylethylenediamine (Sigma Aldrich, T9281), ammonium persulfate (Sigma Aldrich, A3678), and acrylic acid N-hydroxysuccinimide ester (Sigma, A8060) [29]. Using a 20 µL pipette, gel solutions were cast into the wells and allowed to polymerize for 90 minutes. Ammonium persulfate concentrations and NHS concentrations were optimized for an argon atmosphere and are approximately 10x lower than previously published values [29]. The concentrations used typically create a thin, unpolymerized region near the PDMS walls, ensuring that the hydrogel is mechanically isolated from the PDMS well. After polymerization, gels were removed from the glovebox and the 18 mm x 18 mm coverslip was removed and discarded. Gels were stored in PBS overnight and for up to seven days at 4ºC.

Device Characterization

Fabrication of polyacrylamide gel-based systems have previously been shown to be highly controllable and repeatable [30] and previous experimental research [31] and subsequent mechanical models [32] determined that for polyacrylamide gels with thicknesses of >70 µm, the underlying glass substrate does not contribute to the locally measured stiffness. Here, the gels within our microdevice system are consistently >250 µm in thickness (Extended Data Figure 4a)), effectively preventing substrate effects from the underlying glass surface. We also performed

atomic force microscopy measurements to determine the stiffness of the gel constructs. Measurements were performed on polyacrylamide gels in laser cut microchannels using a colloidal cantilever (sQube, CP-PNPL-PS-A) with a stiffness of 0.08 N/m and 1.98 μm diameter polystyrene sphere. Gel stiffnesses were in agreement with our calculated predicted values, and those reported by the literature [33] (Extended Data Figure 4b).

Testing was performed to confirm that the microdot pairs are indeed independent of one another and that a contracting platelet does not affect the mechanics of the neighboring microdot pair. With this system, the displacement field around the applied point force is expected decay over relatively short distances, as predicted by previous work [34]. Here, the microdot pairs are spaced far apart (8 μm or greater) relative to the microdot pair displacement caused by platelet contraction, which is on the order of 1 μm or less. At this distance, displacements induced by neighboring contracting platelets are expected to be negligible. To confirm this, we analyzed the microdot displacements of a single contracting platelet surrounded by empty microdot pairs in real time, and show that movement occurs only in the microdots to which the platelet is attached (Extended Data Figure 4c-d). Some negligible movement may occur below the limit of detection of 0.05 μm, which was determined from measuring peak-to-peak movement in stationary microdots with no adherent platelets in the vicinity.

PDMS microfluidic top

PDMS microfluidics were cast from a SU-8 (Microchem Inc.) mold to create microfluidic channels and sized to cover the hydrogel strips. Microfluidics were 22 mm long x 1.5 mm wide, by 200 μm tall. To assemble, the gels were rinsed with DI water and dried to the extent that all water on the coverslip-PDMS piece was removed. This is greatly facilitated by the fact that the

PDMS remains hydrophobic and the polyacrylamide gels are hydrophilic. The PDMS microfluidic was then quickly attached using a laser cut silicone adhesive (3M, 91022) to ensure that the gels do not dry during assembly. PBS was then flown into the enclosed channels until it was ready for use. The double sided tape approach is unique in that it provides rapid attachment of a microfluidic without affecting the patterned proteins.

Coverslip hybrid microfluidic top

The PDMS microfluidics were best suited to experiments requiring the use of shear flow. For experiments involving static flow conditions, a hybrid lid composed of laser cut PDMS and a coverslip facilitated imaging. Similar to conditions outlined above, premade PDMS sheets (Rogers HT6240-0.01") were laser cut with well patterns, cleaned, and bonded to 18 mm x 18 mm No 1. glass coverslips. Using the same procedure outline in the PDMS microfluidic top, the coverglass and PDMS hybrid lid is bonded to the hydrogel device layer using laser cut silicone adhesive. Upon experimental completion, the ends of the device may be sealed with silicone grease for multi-day storage.

Experimental Methods

Platelet preparation

Healthy blood donors and patient donors had abstained from aspirin in the last two weeks, and consent was obtained according to GT IRB H15258. Blood was drawn by median venipuncture into acid-citrate-dextrose (ACD) solution 2. The sample was subsequently centrifuged at 150 G for 15 min, and the resulting platelet rich plasma was gel filtered into HEPES modified Tyrodes buffer as described previously [35]. Platelets were diluted to a final concentration of 4 x 10^6/mL in Tyrodes buffer to minimize potential paracrine signaling. This equated to an average distance

between microdot pairs of 30-50 microns depending on the donor. In some experiments, platelets were incubated for 1 hour with vehicle (dimethyl sulfoxide, DMSO); ROCK inhibitor Y-27632 at 50 μm (Sigma Y0503), or MLCK inhibitor at 10 μm (Sigma I2764).

For bulk contraction studies, blood was drawn by median antecubital venipuncture into acid-citrate-dextrose (ACD) solution 2. The sample was centrifuged 150 G for 15 min and the resulting platelet rich plasma was collected, and centrifuged with an additional 10% ACD by volume at 900G for 5min. The supernatant, platelet poor plasma, was discarded and the platelets were resuspended into HEPES modified Tyrodes buffer.

Microdevice plating

Immediately prior to loading platelets into the microfluidic the following was added: 5 mM of $CaCl_2$, 5 mM of $MgCl_2$, 3 μg/mL of fibrinogen, thrombin (Haematologic Technologies, Inc), and any relevant inhibitors. The small dimensions of the microfluifidic ensure that platelets rapidly move to the ligand interaction region after activation. After 15 minutes, 60 uL of a wash solution consisting of 5 mM of $CaCl_2$, 5 mM of $MgCl_2$, thrombin, and any relevant inhibitors was used to remove residual platelets from solution. Thrombin both activates the platelets and converts microdot fibrinogen into monomeric fibrin, more closely recapitulating the in vivo environment [17,18]. For some experiment involving shear stress, flow was applied using syringe pumps (PhD Ultra, Harvard Apparatus) with the wash solution to create a shear rates of either $500s^{-1}$ or $1000s^{-1}$. The adhered platelets were then incubated for 90 minutes, which is several times more than needed for contraction to ensure that all platelets had sufficient time to reach a final state of contraction. Platelets were then fixed with a solution of Tyrodes buffer with 4% paraformaldehyde, 5 mM $CaCl_2$, and 5 mM $MgCl_2$ for 15 minutes.

Coverslip preparation & plating

In conditions where a platelet sample was extremely rare (WAS, MYH9-RD), was imaged live, or required later mounting for high resolution imaging, micropatterned gels on 25 mm coverslips were used. Bottom coverslips were prepared by silanized using the method described above, and top coverslips were micropatterned using the technique described above. Gels were then prepared and placed in between the coverslips. Similar plating protocols were used, with the exception that gel coverslips were placed in 6 well plates, and platelet concentrations were dropped to 2M/mL.

Plating optimization:

Platelet behavior is affected by many different behaviors paracrine signaling, ligand density [28], ligand type, and shear stress [11]. The device presented in this paper sought to quantify changes in platelet contraction due to differences in substrate stiffness and thrombin concentration, while holding all other parameters constant.

*ADP***:** Our initial experiments examining the effect of ADP on platelet contraction were inconsistent for the same individuals and over time. Measured forces were much lower than thrombin, but were extremely varied in both platelet adhesion and forces.

Platelet Concentration: Platelet behavior may be affected by nearby activated platelets. To minimize potential confounding effects, the platelet concentration chosen is purposefully low to ensure an average distance between contracting platelets of approximately 30 to 50 microns. There may be some enhancement of platelet contraction by neighboring platelets, but early tests

with and without apyrase found no change in contraction measurements from the presence of apyrase.

Ligand Density: It is possible that order of magnitude changes in ligand density could affect outside-in signaling, as shown earlier [7,28]. We sought to examine this phenomenon but were constrained by the range of ligand densities that can be achieved using this system. Here, 30 μg/mL was optimal, creating well defined, repeatable patterns which supported platelet adhesion. When the stamping solution was 3 μg/mL, platelet adhesion was poor. At 300 μg/mL, the fibrinogen formed sheets which had the propensity to curl, lowering pattern fidelity. Overall, we expect trends presented here to be preserved on different ligand densities in light of previous reports [7] showing mechanosensitive trends are similar in low and high ligand density environments.

Shear Stress: Platelets were incubated for 15 minutes with thrombin concentrations of 0.1 or 1 U/mL on the polyacrylamide gels to ensure adhesion. Shear rates of 500 and 1000 s^{-1} applied for 1.5 hours to each thrombin concentration. Platelets were then fixed under flow with 4% PFA and imaged. No statistically significant differences were observed due to the application of shear stress from static controls at either thrombin concentration. Activating the platelets and allowing them to adhere to the fibrinogen under flow would enable shear stress to be applied during the entire activation process, leading to more firm conclusions that shear does not affect platelet contraction on fibrinogen with thrombin. Unfortunately, this condition is difficult to test as the constant flow of platelets also leads to multi-platelet aggregates.

Immunocytochemistry

After fixation, depending on the experiment, platelets were stained with an appropriate plasma membrane dye (Cell Mask Deep Red or Cell Mask Orange, Life Technologies). In some instances, platelets were counterstained with phallodin (Alexa Fluor conjugated, Life Technologies) or phosphatidylserine with Annexin V (Alexa Fluor conjugated, Life Technologies). For detecting activated $\alpha_{IIb}\beta_3$, FITC-PAC-1 antibody (BD Biosciences) was applied to platelets after 75 minutes.

Imaging & Mounting

Gels were imaged on a Zeiss LSM 700-405 confocal microscope using a 20x 0.8 NA lens. For high resolution images, samples were rinsed with DI water, inverted and mounted onto coverslips (ProLong Gold Antifade, ThermoFisher Scientific). High resolution images of platelets were obtained using a GE Deltavision OMX Blaze using a 100x, 1.49 NA objective.

For high resolution scanning electron microscopy, samples were extracted from microfluidics, and incubated overnight in 50% ionic liquid (IL1000, Hitachi) and 50% deionized water. Excess liquid was wicked away using filter paper. Samples were imaged using a Hitachi SU8230 cold field emission SEM.

Image Analysis

Images were analyzed using a MATLAB script which measured the fibrinogen microdot areas, and calculated the center to center distance of the fibrinogen microdots. Due to the high pattern fidelity, the initial uncontracted distance was taken to be the distance of a neighboring pair of uncontracted microdots. Although minimized, occasional multi-platelet aggregates identifiable

by size occurred and were ignored. The current script and data collection is semi-automated, where confocal images are manually collected, and individual platelet pairs are identified by hand, then subsequently analyzed by the script. Such a system may readily be adapted for automation in future studies.

Bulk Isotonic Clot Contraction

Polystyrene fluorimeter cuvettes (Sigma-Aldrich) with attached grids of 1 mm spacing were incubated with 1% F-127 pluronic (Sigma) at room temperature for 1 hour. A solution consisting of 2 mg/mL of purified human fibrinogen (FIB 3, Enzyme Research Laboratories), and 250 x 10^6 washed platelets/mL was prepared. This platelet-fibrin solution was then combined with 1U/mL of thrombin and 5mM $CaCl_2$ in the cuvette and kept at room temperature. Pictures of clot contraction were taken every 30 minutes, and clot volume was estimated using the attached grid.

Bulk Isometric Rheometry

Rheological measurements were performed with a stress-controlled rheometer (Anton Paar MCR 502) using cone-plate geometry. The clot was formed *in situ* and the shear moduli (G' and G'') as well as the normal force were measured as the clot forms. All measurements were done in the linear regime. Final clots composition consisted of: 2 mg/mL of purified human fibrinogen (FIB 3, Enzyme Research Laboratories), 250 x 10^6 washed platelets/mL, 1U/mL of thrombin, and 1 mM $CaCl_2$.

References

1. Jen, C. J. & McIntire, L. V. The structural properties and contractile force of a clot. *Cell Motil.* **2,** 445–55 (1982).

2. HVAS & Sørensen... Tranexamic acid combined with recombinant factor VIII increases clot resistance to accelerated fibrinolysis in severe hemophilia A. (2007). doi:10.1111/j.1538-7836.2007.02755.x

3. Collet, J. P. *et al.* Altered fibrin architecture is associated with hypofibrinolysis and premature coronary atherothrombosis. *Arterioscler. Thromb. Vasc. Biol.* **26,** 2567–73 (2006).

4. Carr, M. E. Development of platelet contractile force as a research and clinical measure of platelet function. *Cell Biochem. Biophys.* **38,** 55–78 (2003).

5. Cohen, I. & De Vries, A. Platelet contractile regulation in an isometric system. *Nature* **246,** 36–7 (1973).

6. Young, G. *et al.* Thrombin generation and whole blood viscoelastic assays in the management of hemophilia: current state of art and future perspectives. *Blood* **121,** 1944–1950 (2013).

7. Qiu, Y. *et al.* Platelet mechanosensing of substrate stiffness during clot formation mediates adhesion, spreading, and activation. *Proc. Natl. Acad. Sci. U.S.A.* **111,** 14430–5 (2014).

8. Lam, W. A. *et al.* Mechanics and contraction dynamics of single platelets and implications for clot stiffening. *Nat Mater* **10,** 61–6 (2011).

9. Kita, A. *et al.* Microenvironmental geometry guides platelet adhesion and spreading: a quantitative analysis at the single cell level. *PLoS ONE* **6,** e26437 (2011).

10. Stalker, T. J. *et al.* Hierarchical organization in the hemostatic response and its relationship to the platelet-signaling network. *Blood* **121,** 1875–85 (2013).

11. Nesbitt, W. S. *et al.* A shear gradient-dependent platelet aggregation mechanism drives thrombus formation. *Nat. Med.* **15,** 665–73 (2009).

12. Kroll, M. H., Hellums, J. D., McIntire, L. V., Schafer, A. I. & Moake, J. L. Platelets and shear stress. *Blood* **88,** 1525–41 (1996).

13. Weisel, J. W. Biophysics. Enigmas of blood clot elasticity. *Science* **320,** 456–7 (2008).

14. Schwarz Henriques, S., Sandmann, R., Strate, A. & Köster, S. Force field evolution during human blood platelet activation. *Journal of cell science* **125,** 3914–20 (2012).

15. Liang, X. M., Han, S. J., Reems, J.-A. A., Gao, D. & Sniadecki, N. J. Platelet retraction force measurements using flexible post force sensors. *Lab Chip* **10,** 991–8 (2010).

16. Suzuki-Inoue, K. *et al.* Involvement of Src kinases and PLCgamma2 in clot retraction. *Thromb. Res.* **120,** 251–8 (2007).

17. Litvinov, RI, Gorkun, OV, Owen, SF & Shuman, H. Polymerization of fibrin: specificity, strength, and stability of knob-hole interactions studied at the single-molecule level. *Blood* (2005). at <http://www.bloodjournal.org/content/106/9/2944.short>

18. Litvinov, R. I. *et al.* Polymerization of fibrin: direct observation and quantification of individual B: b knob-hole interactions. *Blood* **109,** 130–138 (2007).

19. Engler, A. *et al.* Embryonic cardiomyocytes beat best on a matrix with heart-like elasticity: scar-like rigidity inhibits beating. *J Cell Sci* **121,** 3794–802 (2008).

20. Paszek, M. J. *et al.* Tensional homeostasis and the malignant phenotype. *Cancer Cell* **8,** 241–54 (2005).

21. Burridge, K. & Wittchen, E. The tension mounts: Stress fibers as force-generating mechanotransducers. *The Journal of Cell Biology* **200,** 9–19 (2013).

22. De Gennes, P.-G. *Scaling Concepts in Polymer Physics*. (Cornell University Press).

23. Shah, J. & Janmey, P. Strain hardening of fibrin gels and plasma clots. *Rheol Acta* **36,** 262–268 (1997).

24. Godwin, H. & Ginsburg, D. May□Hegglin Anomaly: A Defect in Megakaryocyte Fragmentation? *British Journal of Haematology* **26,** 117–127 (1974).

25. Shcherbina, A. *et al.* WASP plays a novel role in regulating platelet responses dependent on alphaIIbbeta3 integrin outside-in signalling. *Br. J. Haematol.* **148,** 416–27 (2010).

26. Pedersen, J. A. & Swartz, M. A. Mechanobiology in the third dimension. *Ann Biomed Eng* **33,** 1469–90 (2005).

27. Von Philipsborn, A. C. *et al.* Microcontact printing of axon guidance molecules for generation of graded patterns. *Nat Protoc* **1,** 1322–8 (2006).

28. Jirousková, M., Jaiswal, J. K. & Coller, B. S. Ligand density dramatically affects integrin alpha IIb beta 3-mediated platelet signaling and spreading. *Blood* **109,** 5260–9 (2007).

29. Polio, S. R., Rothenberg, K. E., Stamenović, D. & Smith, M. L. A micropatterning and image processing approach to simplify measurement of cellular traction forces. *Acta Biomater* **8,** 82–8 (2012).

30. Tse, J. R. & Engler, A. J. Stiffness gradients mimicking in vivo tissue variation regulate mesenchymal stem cell fate. *PLoS ONE* **6,** e15978 (2011).

31. Engler, A. J., Sen, S., Sweeney, H. L. & Discher, D. E. Matrix elasticity directs stem cell lineage specification. *Cell* **126,** 677–89 (2006).

32. Maloney, J. M., Walton, E. B., Bruce, C. M. & Van Vliet, K. J. Influence of finite thickness and stiffness on cellular adhesion-induced deformation of compliant substrata. *Phys Rev E Stat Nonlin Soft Matter Phys* **78,** 041923 (2008).

33. Tse, J. R. & Engler, A. J. Preparation of hydrogel substrates with tunable mechanical properties. *Curr Protoc Cell Biol* **Chapter 10,** Unit 10.16 (2010).

34. Sabass, B., Gardel, M., Waterman, C. & Schwarz, U. High Resolution Traction Force Microscopy Based on Experimental and Computational Advances. *Biophys J* **94,** 207–220 (2008).

35. McCabe White, M. & Jennings, L. K. *Platelet Protocols: Research and Clinical Laboratory Procedures*. (Academic Press).

36. Gersh, K. C., Nagaswami, C. & Weisel, J. W. Fibrin network structure and clot mechanical properties are altered by incorporation of erythrocytes. *Thromb. Haemost.* **102,** 1169–75 (2009).

37. Collet, J.-P. P., Shuman, H., Ledger, R. E., Lee, S. & Weisel, J. W. The elasticity of an individual fibrin fiber in a clot. *Proc. Natl. Acad. Sci. U.S.A.* **102,** 9133–7 (2005).

End Notes:

Supplementary Information is linked to the online version of the paper

Acknowledgements: The authors wish to thank Andrew Shaw of the Parker H. Petit Institute for Bioengineering and Bioscience at the Georgia Institute of Technology (GT); the Emory University Integrated Cellular Imaging Microscopy Core of the Children's Pediatric Research Center; and the GT Institute for Electronics and Nanotechnology (IEN) cleanroom. Financial support provided by NIH R01 (HL121264) to WAL, an AHA Postdoctoral Fellowship to DRM. DRM thanks CRD and GAK for comments and discussion.

Author Contributions: DRM & WAL conceived of and designed platelet contraction experiments. DRM, YQ, ACB, JC, BA, MS, TS, & WAL designed and tested platelet contraction cytometer. DRM, YS, RT, RM, SB, CB, MB performed experiments. MEF designed and wrote image analysis algorithms. DRM & WAL analyzed data and wrote the manuscript.

Author Information:. The authors declare no competing financial interests. Correspondence and requests for materials should be addressed to wilbur.lam@emory.edu

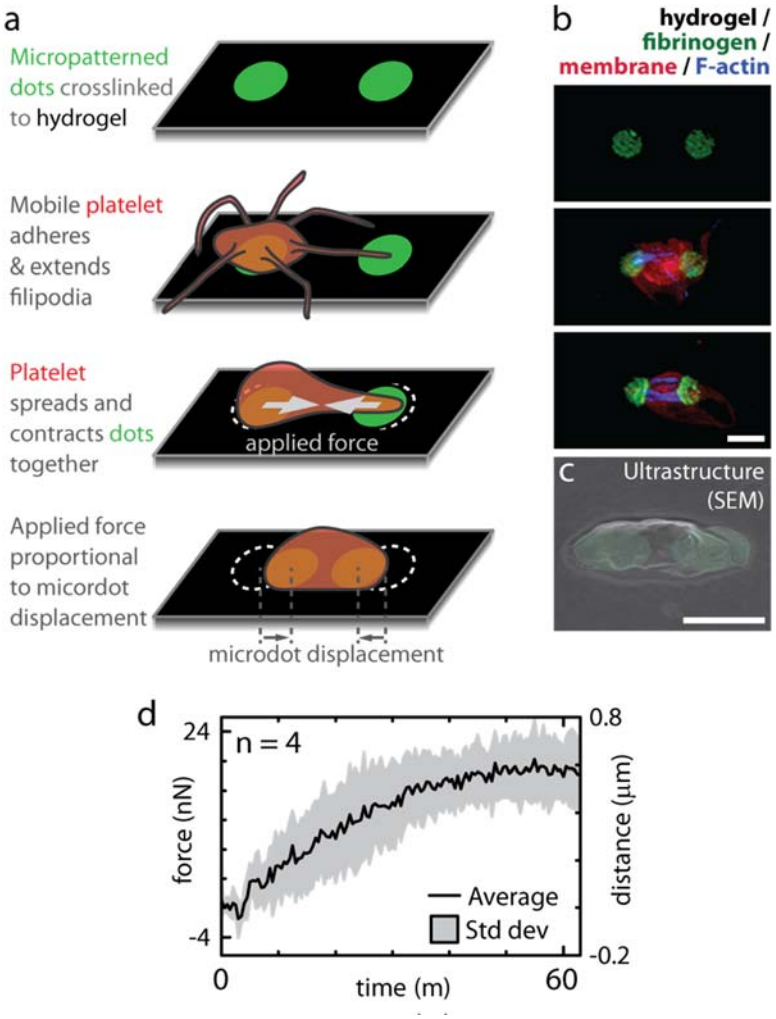

523

524 Figure 1: The fundamental unit driving clot stiffening, a single platelet pulling against a
525 fibrin/ogen substrate, is established by recapitulating the mechanical and biological
526 microenvironment of the platelet. **a,** Fluorescently-conjugated fibrinogen microdot pairs are
527 covalently bound to a deformable polyacrylamide hydrogel of known mechanical properties. As
528 a platelet adheres and pulls pairs of fibrinogen microdots together, the contractile force is
529 proportional to the microdot displacement. **b,** Super-resolution microscopy images of individual
530 platelets with various degrees of contraction, scale bar is 2 μm **c,** Scanning electron microscopy
531 image of a platelet contracting a fibrinogen microdot pair, scale bar is 2 μm. **d,** Real time
532 contractile measurements of 4 single platelets.

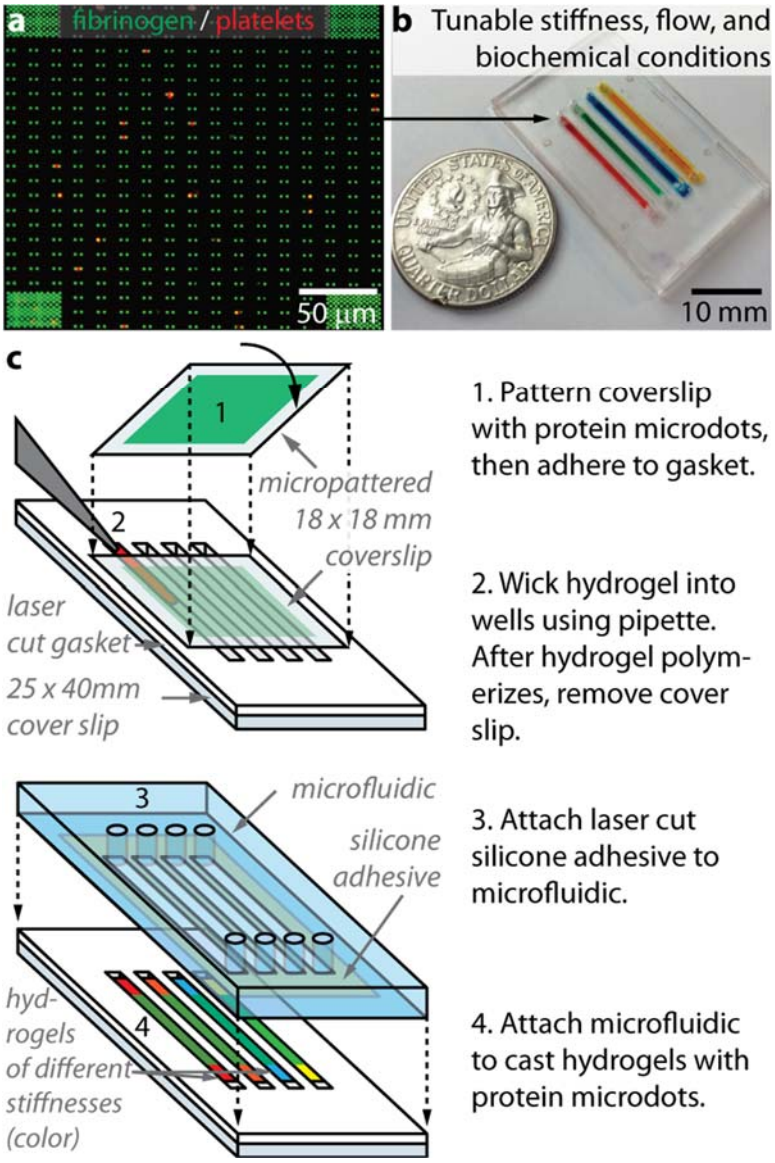

Figure 2: Platelet contraction cytometer - hydrogels with microprinted arrays of fibrinogen microdots are encapsulated in separate microchannels, enabling the biochemical, mechanical, and shear microenvironments to be precisely controlled and varied simultaneously. **a,** A confocal image showing single platelets (red, contracting against fibrinogen microdot pairs (green) on the hydrogel surface. Over 20,000 fibrinogen microdot pairs are microprinted on the surface of each hydrogel encapsulated in each microchannel. **b,** Each microfluidic device may comprise different variables,, here four of microchannels comprise of hydrogels of different stiffness. **c,** A novel yet relatively simple fabrication process flow enables rapid manufacturing.

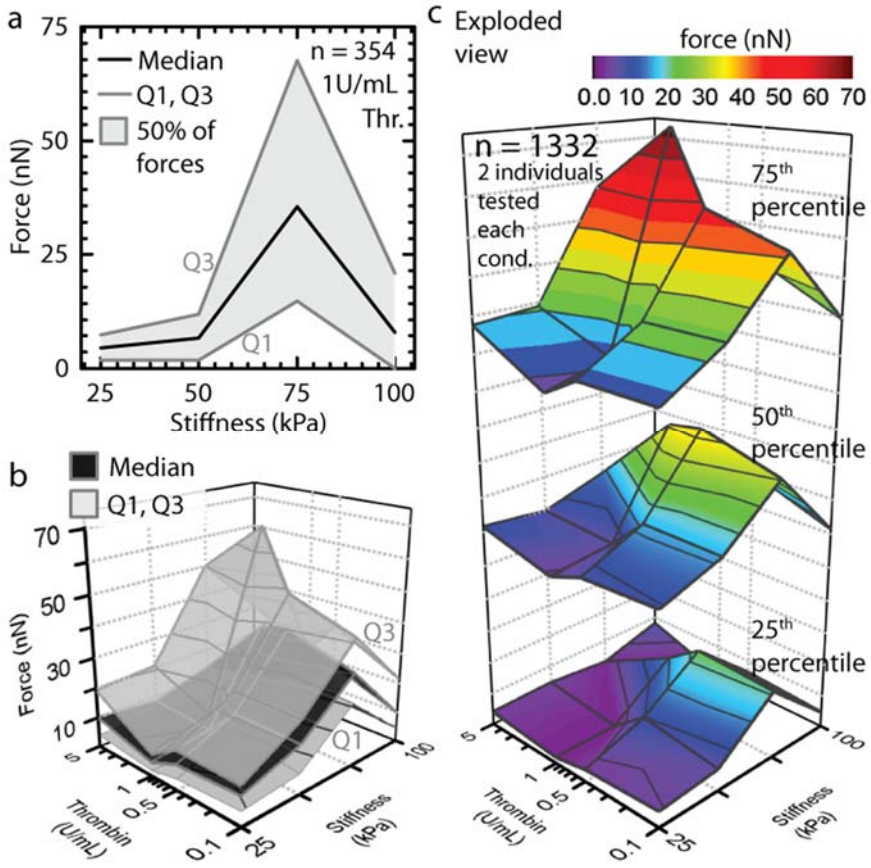

Figure 3: Biochemical and mechanical cues synergistically mediate platelet contraction force. **a,** Maximal platelet contraction occurs at 75kpa substrate stiffness and 1U/mL thrombin. **b,** Single platelet force quartiles for physiologically relevant clot stiffnesses and thrombin concentrations. Platelet contractile forces are highest at a substrate stiffness of 75 kPa or at 5U/mL thrombin. A minimum occurs at 25 kPa stiffness and 1U/mL thrombin. **c,** Exploded view of b to aid visualization. Microenvironmental stiffness has a dominant role over thrombin concentration. Force attenuation at the highest stiffness conditions suggests a mechanically mediated negative feedback mechanism governing the upper limits of platelet contraction. n refers to total number of platelets tested.

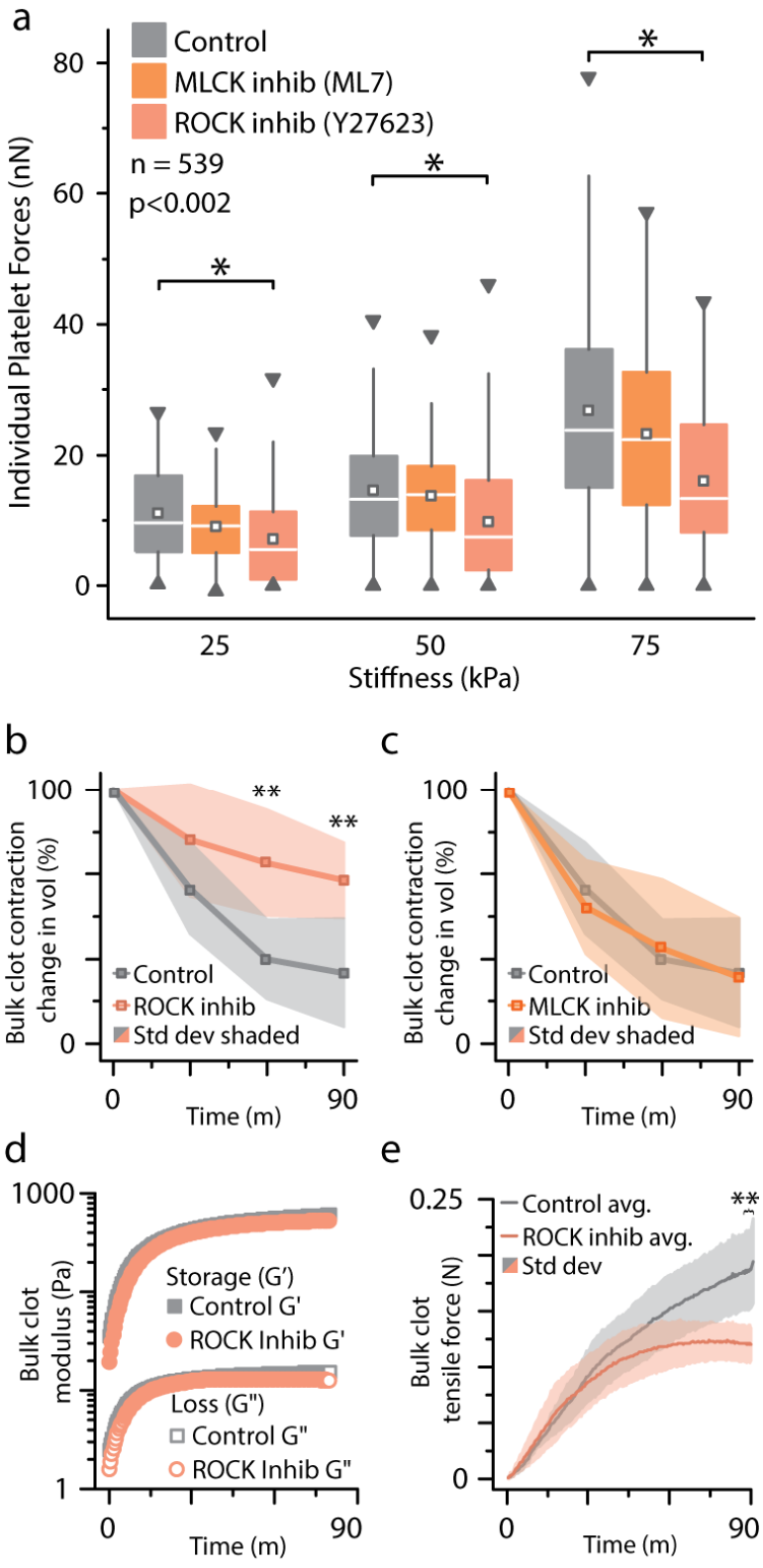
a
Control
MLCK inhib (ML7)
ROCK inhib (Y27623)
n = 539
p<0.002
Individual Platelet Forces (nN)
Stiffness (kPa)
25
50
75
b
Bulk clot contraction change in vol (%)
Control
ROCK inhib
Std dev shaded
Time (m)
c
Control
MLCK inhib
Std dev shaded
Time (m)
d
Bulk clot modulus (Pa)
Storage (G')
Control G'
ROCK Inhib G'
Loss (G")
Control G"
ROCK Inhib G"
Time (m)
e
Bulk clot tensile force (N)
Control avg.
ROCK inhib avg.
Std dev
Time (m)

552

Figure 4: Mechanotransductive platelet contraction is mediated by the Rho-associated protein kinase (ROCK) pathway, as measured with platelet contraction cytometry and standard bulk clot contraction and bulk clot rheometry. **a,** The increase in platelet contractile forces with increasing substrate stiffness is significantly reduced with exposure to Y27623, a pharmacologic ROCK inhibitor. Pharmacologic inhibition of the myosin light chain kinase (MLCK) with ML7, on the other hand, did not produce a statistically significant difference in the substrate stiffness-mediated effect on platelet contractile force. Box denotes median and quartiles; whiskers to 1.5 interquartlie range), square denotes median, triangles denotes 1% and 99%. (n = 539, each condition n>40). * indicates differences from control at same stiffness ($p < 0.05$ by Mann-Whitney). **b,** ROCK inhibition impairs bulk clot contraction (n = 4) as compared to the untreated control clots. **c,** MLCK inhibition does not change bulk clot contraction (n = 4). **d,** Oscillatory rheometry, which enables simultaneous measurements of storage and loss moduli as well as bulk tensile forces, revealed that both control and ROCK-inhibited clots undergo a dramatic stiffening process (representative plot from 3 similar experiments shown). The angular frequency and strain amplitude are 1 rad/s and 0.01, respectively, which are well within the linear regime of the samples. **e,** Control and ROCK-inhibited clots apply similar forces during the beginning of clot formation when the measured storage and loss moduli are low (n = 3). As the clots stiffen (Figure 4d), ROCK-inhibited bulk clots begin to exert lower tensile forces and plateau while the control continues to increase over time. ** indicates difference from control ($p < 0.05$ by t-test).

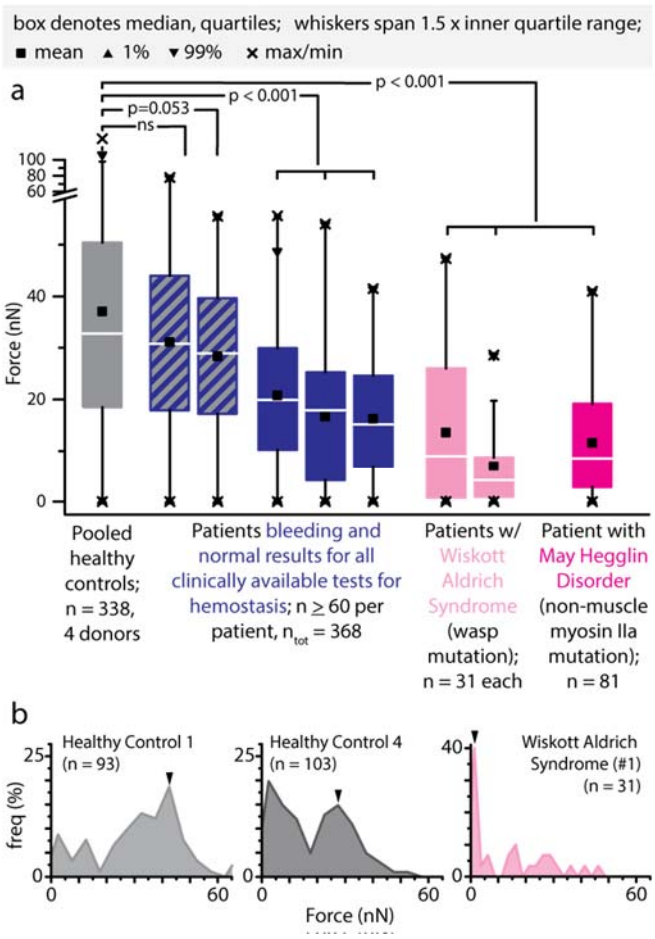

572

573 Figure 5: Patients with phenotypic bleeding lack highly contractile platelets associated with clot
574 contraction and force generation. **a,** Wiskott Aldrich Syndrome and May Hegglin Disorder
575 platelets exhibited significantly reduced contractile forces compared to that of healthy controls
576 (75 kPa gel stiffness, 1U/mL thrombin). In a subset of patients with bleeding diatheses yet
577 normal hemostasis tests, platelet contraction was lower than that of normal healthy controls.
578 **b,** Histogram data reveal platelet subpopulations of varying contractile forces. Healthy control
579 platelets comprise high contractility subpopulations, notably absent in platelets from a Wiskott
580 Aldrich Syndrome patient. In all panels, n refers to number of platelets, Mann-Whitney statistical
581 test.

582 **Figure Legends**

583 Figure 1: The fundamental unit driving clot stiffening, a single platelet pulling against a
584 fibrin/ogen substrate, is established by recapitulating the mechanical and biological
585 microenvironment of the platelet. **a,** Fluorescently-conjugated fibrinogen microdot pairs are
586 covalently bound to a deformable polyacrylamide hydrogel of known mechanical properties. As
587 a platelet adheres and pulls pairs of fibrinogen microdots together, the contractile force is
588 proportional to the microdot displacement. **b,** Super-resolution microscopy images of individual
589 platelets with various degrees of contraction, scale bar is 2 μm **c,** Scanning electron microscopy
590 image of a platelet contracting a fibrinogen microdot pair, scale bar is 2 μm. **d,** Real time
591 contractile measurements of 4 single platelets.

592 Figure 2: Platelet contraction cytometer - hydrogels with microprinted arrays of fibrinogen
593 microdots are encapsulated in separate microchannels, enabling the biochemical, mechanical,
594 and shear microenvironments to be precisely controlled and varied simultaneously. **a,** A confocal
595 image showing single platelets (red, contracting against fibrinogen microdot pairs (green) on the
596 hydrogel surface. Over 20,000 fibrinogen microdot pairs are microprinted on the surface of each
597 hydrogel encapsulated in each microchannel. **b,** Each microfluidic device may comprise different
598 variables,, here four of microchannels comprise of hydrogels of different stiffness. **c,** A novel yet
599 relatively simple fabrication process flow enables rapid manufacturing.

600 Figure 3: Biochemical and mechanical cues synergistically mediate platelet contraction force. **a,**
601 Maximal platelet contraction occurs at 75kpa substrate stiffness and 1U/mL thrombin. **b,** Single
602 platelet force quartiles for physiologically relevant clot stiffnesses and thrombin concentrations.
603 Platelet contractile forces are highest at a substrate stiffness of 75 kPa or at 5U/mL thrombin. A
604 minimum occurs at 25 kPa stiffness and 1U/mL thrombin. **c,** Exploded view of b to aid

visualization. Microenvironmental stiffness has a dominant role over thrombin concentration. Force attenuation at the highest stiffness conditions suggests a mechanically mediated negative feedback mechanism governing the upper limits of platelet contraction. n refers to total number of platelets tested.

Figure 4: Mechanotransductive platelet contraction is mediated by the Rho-associated protein kinase (ROCK) pathway, as measured with platelet contraction cytometry and standard bulk clot contraction and bulk clot rheometry. **a,** The increase in platelet contractile forces with increasing substrate stiffness is significantly reduced with exposure to Y27623, a pharmacologic ROCK inhibitor. Pharmacologic inhibition of the myosin light chain kinase (MLCK) with ML7, on the other hand, did not produce a statistically significant difference in the substrate stiffness-mediated effect on platelet contractile force. Box denotes median and quartiles; whiskers to 1.5 interquartlie range), square denotes median, triangles denotes 1% and 99%. (n = 539, each condition n>40). * indicates differences from control at same stiffness ($p < 0.05$ by Mann-Whitney). **b,** ROCK inhibition impairs bulk clot contraction (n = 4) as compared to the untreated control clots. **c,** MLCK inhibition does not change bulk clot contraction (n = 4). **d,** Oscillatory rheometry, which enables simultaneous measurements of storage and loss moduli as well as bulk tensile forces, revealed that both control and ROCK-inhibited clots undergo a dramatic stiffening process (representative plot from 3 similar experiments shown). The angular frequency and strain amplitude are 1 rad/s and 0.01, respectively, which are well within the linear regime of the samples. **e,** Control and ROCK-inhibited clots apply similar forces during the beginning of clot formation when the measured storage and loss moduli are low (n = 3). As the clots stiffen (Figure 4d), ROCK-inhibited bulk clots begin to exert lower tensile forces and plateau while the control continues to increase over time. ** indicates difference from control ($p < 0.05$ by t-test).

Figure 5: Patients with phenotypic bleeding lack highly contractile platelets associated with clot contraction and force generation. **a,** Wiskott Aldrich Syndrome and May Hegglin Disorder platelets exhibited significantly reduced contractile forces compared to that of healthy controls (75 kPa gel stiffness, 1U/mL thrombin). In a subset of patients with bleeding diatheses yet normal hemostasis tests, platelet contraction was lower than that of normal healthy controls. **b,** Histogram data reveal platelet subpopulations of varying contractile forces. Healthy control platelets comprise high contractility subpopulations, notably absent in platelets from a Wiskott Aldrich Syndrome patient. In all panels, n refers to number of platelets, Mann-Whitney statistical test.

Extended Data Videos

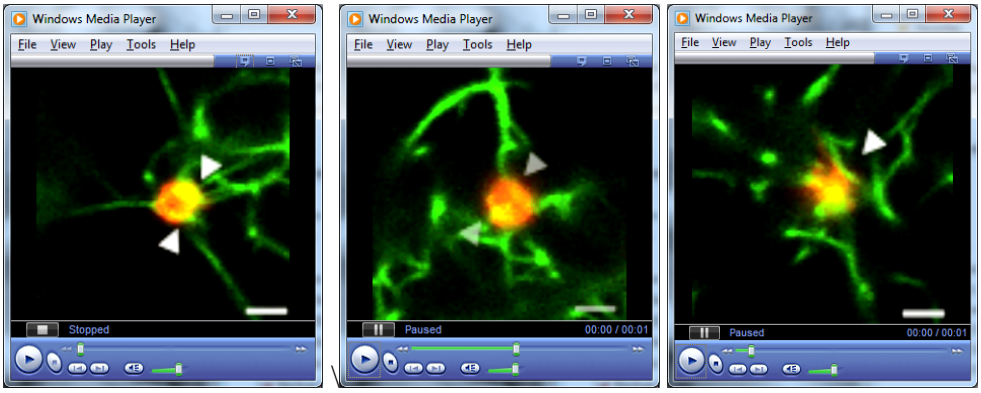

Extended Data Video 1-3: Platelet contraction in 3d fibrin meshes span and pull adjacent fibers together of differing stiffness. The fibrin mesh has varying mechanical stiffness due to the differing thickness and cross linking point density. Here we show three platelets spanning fibrin filaments and pulling them together over the course of six minutes. White arrows point to same feature at both time points. Scale bar is 2 μm.

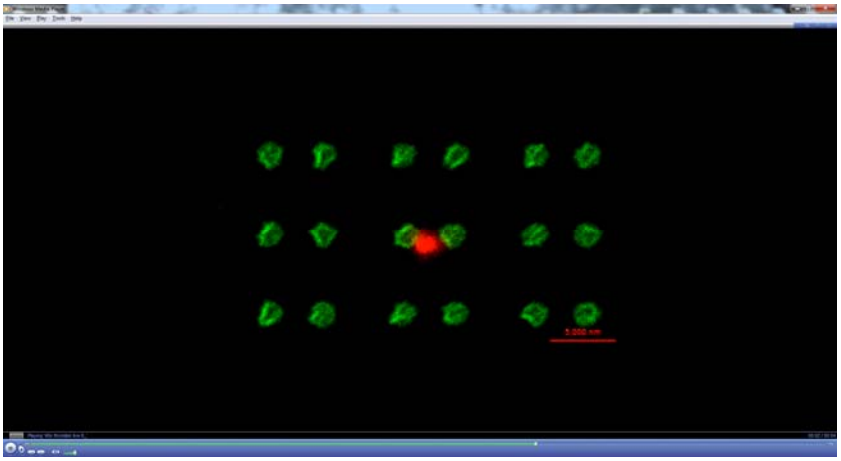

Extended Data Video 4: Individual contracting platelet - A single contracting platelet is imaged during the contraction process. Time elapsed for entire video is 60 minutes.

Extended Data Figures

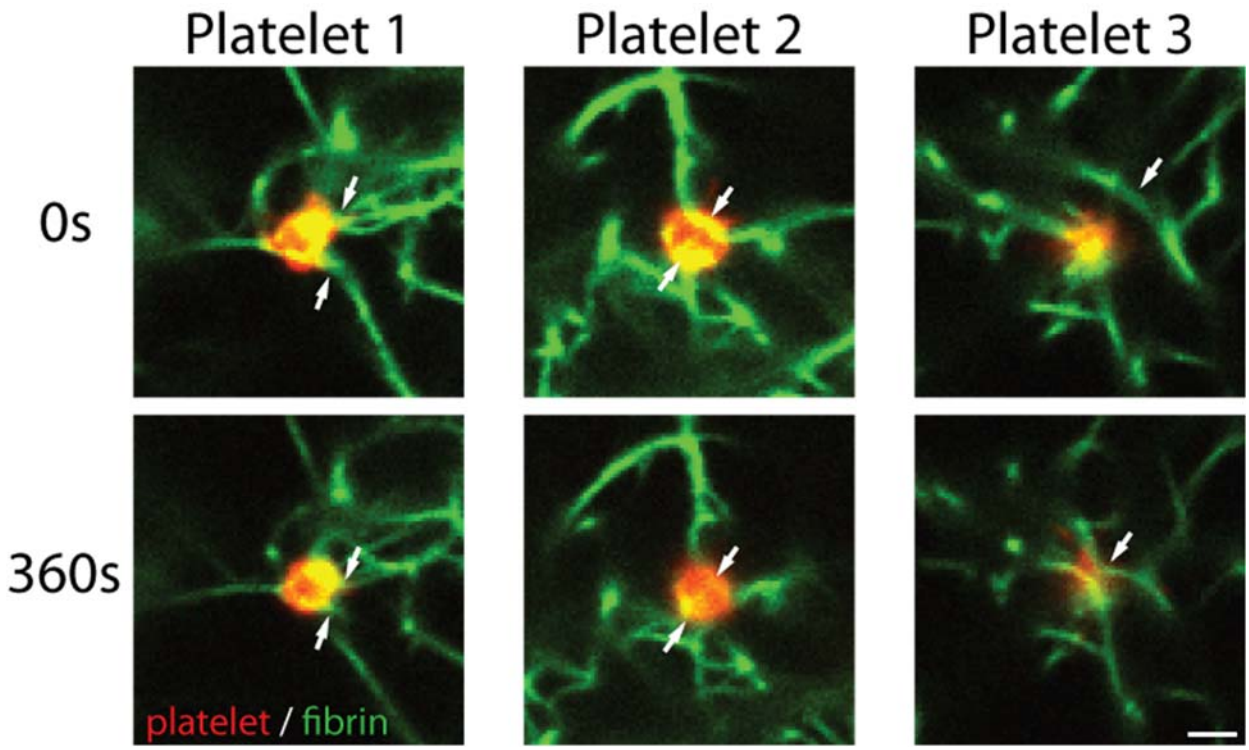

Extended Data Figure 1: Platelet contraction in 3d fibrin meshes span and pull adjacent fibers together of differing stiffness. The fibrin mesh has varying mechanical stiffness due to the differing thickness and cross linking point density. Here we show three platelets spanning fibrin filaments and pulling them together over the course of six minutes. White arrows point to same feature at both time points. Scale bar is 2 μm.

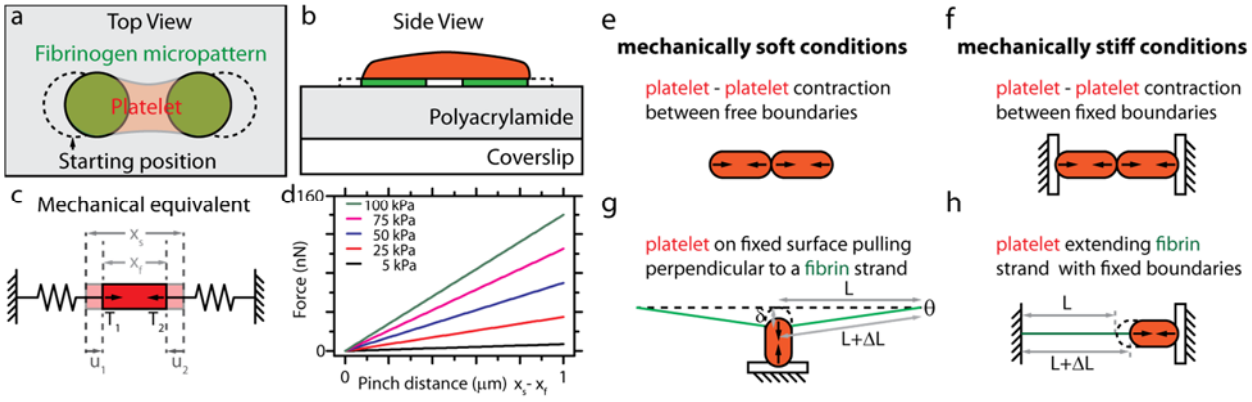

Extended Data Figure 2: Contractile system, mechanical model, and calculated forces as a function of pinch distance, and limiting cases for stiffness. **a-b,** The fibrinogen patches are covalently attached to the underlying hydrogel and move independently. **c,** Mechanically, this can be modeled as a platelet pulling on two springs of equivalent stiffness. **d,** The force a platelet will exert by pulling the fibrinogen patches together may be calculated from a measurement of the pinch distance for a range of different hydrogel stiffnesses. When considering force range, it is important to consider the limiting cases defining mechanical stiffness values **e,** Platelets contracting against one another with moving boundaries are expected to have stiffness on the order of 10 kPa, the value for an activated contracted platelet. **f,** Platelets contracting in between fixed boundaries experience isometric contraction. Previous measurements in isometric contractile conditions found maximal forces of 80nN. **g,** Platelets pulling a fibrin strand perpendicular to the principle axis will cause minimal extension of the fibrin, exerting single nanonewton forces. **h,** Platelets which extend a single fibrin fiber will need to exert several 10s of nanonewtons. Neither g nor h consider pre-strain in the fibrin or multiple fibers which will make the conditions much stiffer.

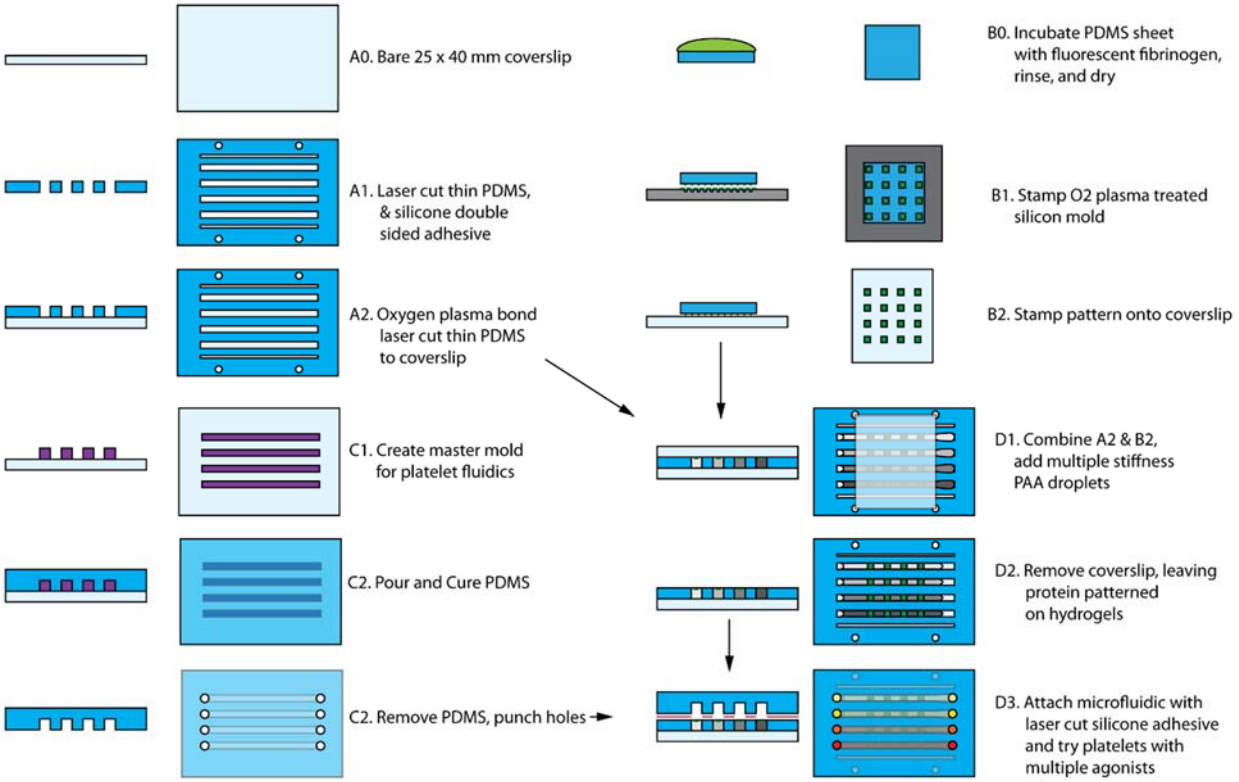

672

673 Extended Data Figure 3: Detailed process flow for construction of microfluidic traction force
674 microscopy test device. Due to the commercial availability of most starting materials, batches of
675 devices may be made in less than 8 hours.

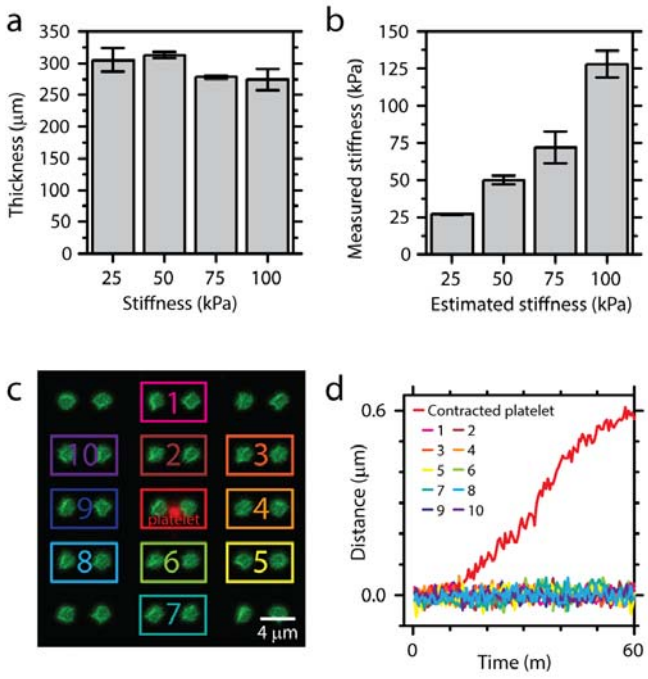

676

677 Extended Data Figure 4: Cast polyacrylamide gels in laser cut gaskets are equivalent to macro
678 systems and enable independent measurements of platelet contractile forces. **a,** Measurements of
679 polyacrylamide gels in channels demonstrate that gels are thicker than 70 µm to ensure that the
680 underlying glass substrate does not contribute to the locally measured stiffness (n = 4, error bars
681 show standard deviation). **b,** The measured stiffness values are in agreement with estimated
682 values, and similar to previously published values in the literature. (n = 18 from two different
683 gels, error bars show standard deviation) **c-d,** A single contracting platelet on a microdot pair
684 does not affect the displacement of the surrounding microdot pairs, demonstrating that each
685 microdot pair is independent from the neighbor.

686

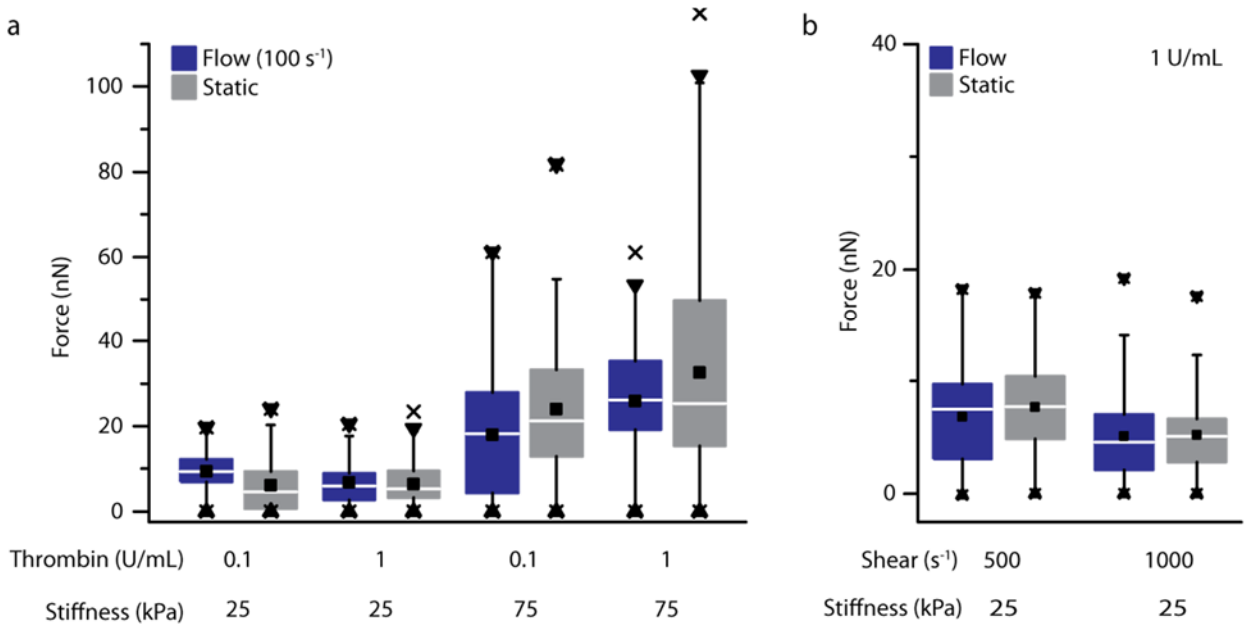

Extended Data Figure 5: Application of shear stress after the initiation of adhesion and contraction has no statistical change on platelet contractile forces. (a) Shear flow was applied at 100 s^{-1} with differing stiffness and thrombin concentration (b) Differing shear was applied at 25 kPa and 1 U/mL thrombin. ($n_{condition} \geq 35$, $n_{total} = 887$)

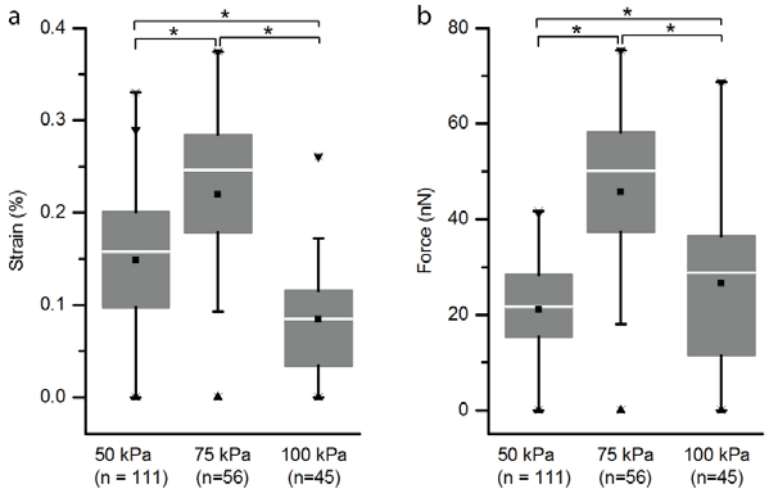

694

695 Extended Data Figure 6: Platelet microdot displacement and force is reduced as the
696 environmental stiffness increases. **a,** Measured microdot displacements become small when the
697 environmental stiffness is very high at 100 kPa. **b,** When converted to force, the distances
698 measured in (a) reveal that a similar range of forces is seen between 75 kPa and 100 kPa stiffness
699 gels, but that the average force is lower, indicating that on average platelets do not apply high
700 contraction forces efficiently in very high stiffness environments. Significance by Mann-
701 Whitney, $\alpha < 0.05$.

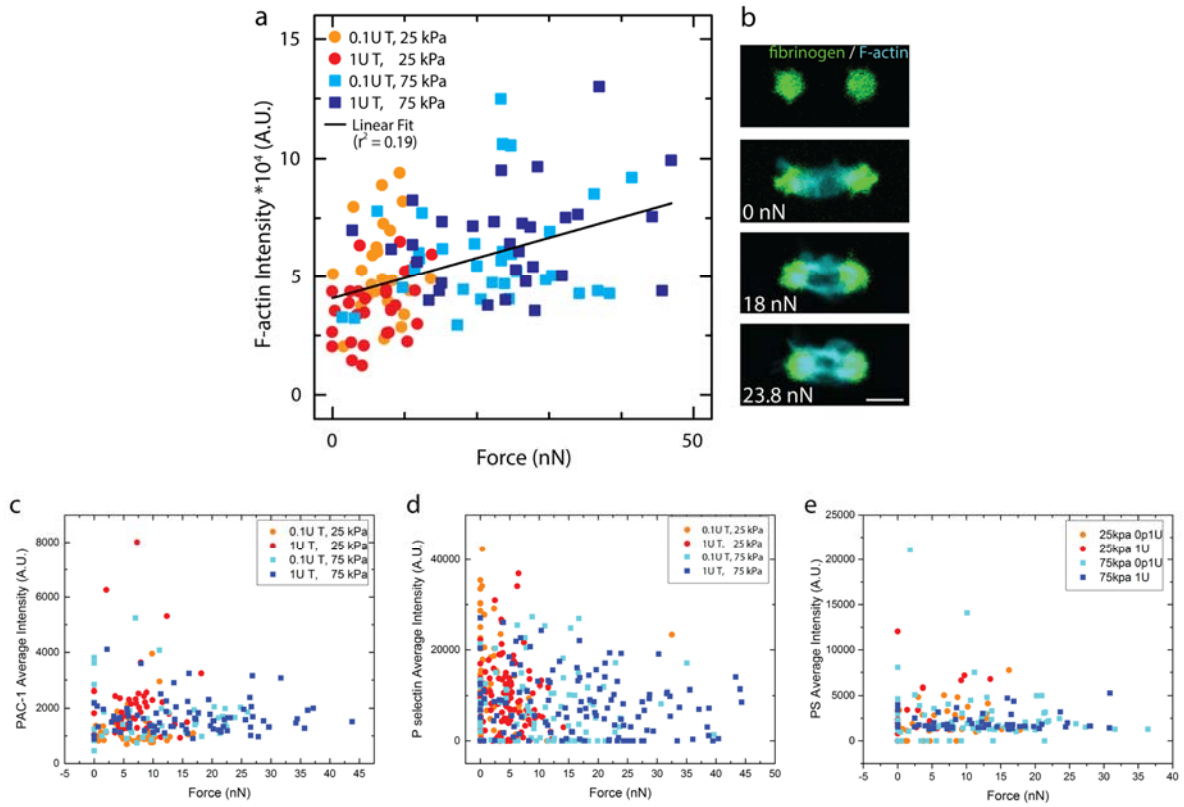

Extended Data Figure 7: F-actin intensity weakly correlates with platelet contractile force, and no discernable correlation is seen with other markers of platelet activation. **a,** F-actin content weakly correlates with contractile force in a variety of different thrombin and mechanical conditions. Correlation of $r > 0.3$ at $\alpha = 0.05$. **b,** Selected images of a separate experiment with 0.1 U/mL thrombin and 25 kPa of some platelets showing increase and improved organization in F-actin with increasing contractile force. As indicated in a, there were also some platelets which did not follow this trend. Little to no correlation in force and **c,** PAC-1 binding, **d,** P-selectin binding, or **e,** PS exposure was observed.

712

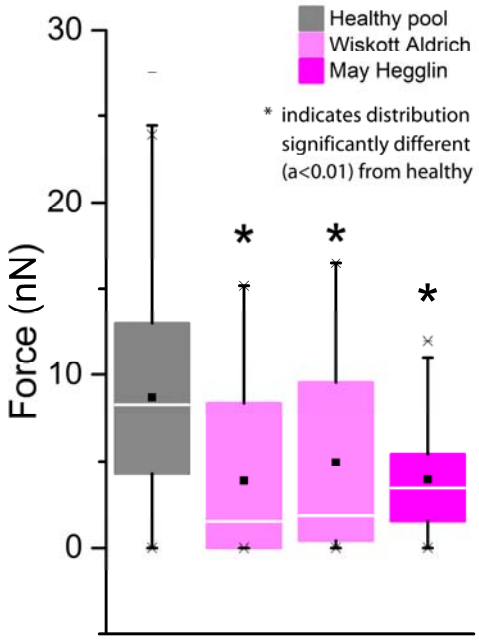

713

714 Extended Data Figure 8: Platelet contractile forces are impaired in individuals with acto-myosin

715 related cytoskeletal mutations on soft gels. ($n_{patient} \geq 28$, $n_{total} = 598$)

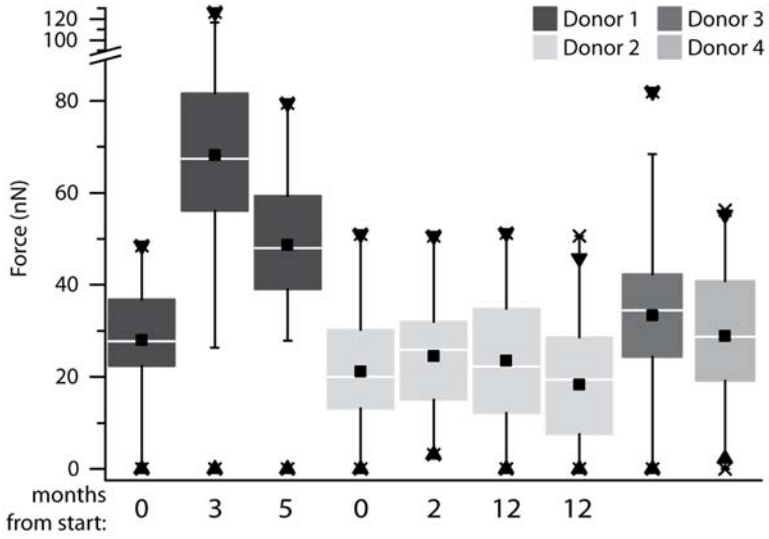

Extended Data Figure 9: Platelet contraction for the same donor over time with numbers indicating time from start. Donor 1 and donor 2 defined the limits of the contraction range measured for healthy individuals, with donor 1 having a high variability in between measurements and donor 2 having exceptionally low variability in between measurements. Donors 3 and 4 were measured at a later time point in the study. ($n_{patient} \geq 30$, $n_{total} = 616$)

Study ID	Contractile force	Bleeding history	Plt count (10^3/uL)	PT (s)	aPTT (s)	fibrinogen (mg/dL)	Factor VIII assay (%)	VWF Ag (%)	Ristocetin cofactor	thrombin time (s)
WL05		easy bruising, spontaneous hematomas, hematuria, occasional nosebleeds	210	13.5	30.6	307	137	107	107	16.8
WL02		heavy menstruation, easy bruising and gum bleeding	229	14	28.9	255	134	96	62	14.9
WL06	low	frequent prolonged nosebleeds, gum bleeding	245	14.6	29.5	330	127	79	78	16.4
WL07	low	frequent nosebleeds	348	14.3	29.2	227	163	165	81	19.3
WL03	very low	heavy menstruation, easy bruising, frequent gum bleeding and nosebleeds	240	13.3	29.9	343	183	60	54	16.4

Extended Data Table 1: Patient history and labs for individuals with unknown bleeding disorders

Study ID	Contractile force	Platelet aggregation interpretation by hematopathologist	PFA
WL05		normal platelet aggregation and release with ADP, arachadonic acid, collagen, ristocetin (low and high dose), thrombin	closure time with collagen/epi - 106 s (normal:83-163 s) and collagen/ADP - 73 s (normal:72-111 s)
WL02		normal platelet aggregation and release with ADP, arachadonic acid, collagen, ristocetin (low and high dose), thrombin	closure time with collagen/epi - 243 s (normal:83-163 s) and collagen/ADP - 174 s (normal:72-111 s) but Hct at 19.4
WL06	low	normal platelet aggregation and release with ADP, arachadonic acid, collagen, ristocetin (low and high dose), thrombin	closure time with collagen/epi - 116 s (normal:83-163 s) and collagen/ADP - not reported (normal:72-111 s)
WL07	low	Mildly decreased aggregation to low and high dose collagen, with normal ATP release. Given all other agonists are normal, this finding likely is clinically insignificant. Repeat testing may be performed if clinically indicated	closure time with collagen/epi - 107 s (normal:83-163 s) and collagen/ADP - 68 (normal:72-111 s)
WL03	very low	normal platelet aggregation and release with ADP, arachadonic acid, collagen, ristocetin (low and high dose), thrombin	closure time minimally elevated with collagen/epi - 177 s (normal:83-163 s) and collagen/ADP - 116 s (normal:72-111 s)

Extended Data Table 2: Interpretation of history and labs for individuals with unknown bleeding disorders by hemopathologist with PFA data

Device design: Mechanics

Surface traction force microscopy

By constraining lithographically patterned arrays of fluorescently tagged proteins to a polyacrylamide gel surface, the computational and experimental constraints of traditional traction force microscopy are greatly reduced [29]. As cells adhere and move protein microdots, the independent traction force, **T**, is calculated as:

$$\boldsymbol{T} = \frac{2\pi G a \boldsymbol{u}}{2 - \nu}$$

where G is the shear modulus, a is the microdot radius, ν is Poisson's ratio, and **u** is the displacement vector. By measuring the displacement of the microdot relative to the starting position, the applied force is calculated. Since the shear modulus of polyacrylamide gels may be changed by changing the ratios of precursor materials [33], the mechanical stiffness felt by the platelet may be changed independent of other parameters such as the ligand area and density.

Simplification of traction force microscopy with two microdot system

Noting that in fibrin clots, platelets may span and pull together two surfaces (Extended Data Figure 1), the method above may be simplified even further by spatially separating microdots such that platelets preferentially attach to two microdots (Extended Data Figure 2a-b). Here, since the gel stiffness is constant, each microdot may be treated as a spring of equivalent stiffness, k, displaced from an equilibrium position u_1 or u_2, as long as the microdot areas are approximately equal (Extended Data Figure 2c). By static equilibrium, $u_1=u_2$, and the displacement of each microdot is:

$$u_1 = u_2 = \frac{1}{2}(x_s - x_f)$$

where x_s is the starting distance of the microdots, and x_f is the final distance of the microdots. The traction force applied by the platelet is the sum of the applied traction forces and may be rewritten in terms of starting distance and final distance.

$$T = T_1 + T_2 = \frac{2\pi G a\, u_1}{2-\nu} + \frac{2\pi G a\, u_2}{2-\nu} = \frac{2\pi G a}{2-\nu}(x_s - x_f)$$

By rewriting the equations in this form, image post-processing is greatly simplified as only two measurements are needed: the final contracted distance and the original uncontracted distance. Using this equation, the force as a function of pinch distance may be calculated for a variety of different gel stiffnesses (Extended Data Figure 2d). Due to the high precision lithography used here, the uncontracted distance may be assumed to be the distance of a neighboring unperturbed pair of microdots, and all measurements are performed once the experiment is completed.

Ligand size choice and spacing

Using a micropatterning [29] approach to traction force microscopy, both ligand area, ligand density, and sytem stiffness could be independently controlled and tuned to mimic geometries and mechanical stiffnesses experienced in clots. In consideration of the platelet size and mindful of lithography and fabrication minimum feature size constraints, we created pairs of fibrinogen circular microdots with a radius of 0.8 μm, and center to center distance of 4 μm (Figure 1). These numbers are similar to those seen in previous AFM studies showing that platelets spread to an area of approximately 1 μm^2 when pulling together two fibrinogen coated surfaces [8], with

microdot displacements of approximately 0.5 – 1 μm. Such numbers also appeared to be in agreement with our own images of platelets contracting in fibrin gels (Extended Data Figure 1, Extended Data Video 1). By spacing pairs of microdots least 8 μm apart[8], platelet contraction was effectively confined to a single pair of microdots (Figure 1b)[9].

The size of the microdots was an important parameter in confining the platelet interaction to two microdots. Platelets are less likely to span to a neighboring microdot when the microdot is large, whereas platelets may span many microdots if the microdots are small and closer together. Aside from creating an appropriate spatial geometry to interact with platelets, the microdot size is also appropriate for optical microscopy. Similarly, based on our force calculations, the microdot size is of an appropriate size to confer adequate force sensitivity and resolution. It is important to note that since the microdot is also a signaling molecule for platelet contraction via $\alpha_{IIb}\beta_3$, that changes in the size could affect platelet behavior. However, any changes in platelet behavior due to a limited ligand area will be systemic since the ligand area is constant for all experiments. Moreover, the data is in agreement with previous atomic force microscopy studies[8], which did not constrain ligand area. Also, since the ligand area also matches *in vitro* clot observations, any errors are expected to be minimal.

After establishing a system of appropriate spatial dimensions, we sought to ensure that the stiffness encountered by platelets was similar to those found in clots. At the single platelet level, this system is expected to be an analog for either platelet-platelet interactions or platelet-fibrin interactions, which are the primary interactions within a clot. A large variety of mechanical stiffnesses are encountered within clots, which have bulk elastic moduli between 45 – 70 Pa[36]. Activated contracted platelets have stiffness values of ~10 kPa[7]; whereas individual fibrin fibers

have stiffness values of 2 MPa (unligated) or 14.5 MPa (ligated) [37]. Using such values it is possible to factor local geometric considerations to estimate the mechanical stiffness and forces that platelets are likely to encounter within a clot. Here the goal is to choose an appropriate range of PAA gel stiffnesses for use within our system. As such, these estimates will focus on limiting cases for the mechanical environment surrounding platelets. This analysis could be carried forth from many different perspectives, but here, expected forces on platelets will be calculated and compared to values achievable with this system (Extended Data Figure 2c)

For platelet-platelet interactions, two limiting cases are considered: when contracting platelets have free boundaries (Extended Data Figure 2e) and when contracting platelets have fixed boundaries (Extended Data Figure 2f). The free boundary case represents the softest interaction which could be experienced by platelet-platelet interactions. In the simplified case, platelets are free to contract and will apply no force to do so. Practically, the material properties of individual platelets will play a dominant role in defining the stiffness of the system. Previous AFM studies have determined that activated, contracted platelets have stiffness of 10 kPa [8]. Hence, forces associated with such systems are expected to be low on the order of several nN. The fixed boundary case represents an interaction in an infinite stiffness environment, where platelets experience isometric contraction. Previous studies have already studied such cases and determined that contractile forces tend to maximum around 80 nN [8]. Our fibrinogen microdots must move in order for contraction to be measured, so PAA gel stiffnesses were chosen which would enable platelets to achieve similar forces with less than 1 μm of contraction. Here, both 75 kPa and 100 kPa gel stiffness meet this criteria (Extended Data Figure 2d).

For platelet-fibrin interactions, the limiting cases are defined by the direction in which a platelet pulls on a single fibrin strand, either perpendicular (Extended Data Figure 2g) or parallel

(Extended Data Figure 2h). Using atomic force microscopy and fibrin fibers spanned across gaps, others have demonstrated that tension built in fibrin networks is through extension of the fibrin and not applied moments. Using published values [37] for typical ligated fibrin diameters (284 ± 44 nm), lengths (14.7 ± 2.5 μm), and modulus (14.5 ± 3.5 MPa), the forces associated with these two conditions may be estimated.

When the platelet pulls perpendicular to the fibrin strand the extension is minimal representing the limit of the soft mechanical environment. Here, assuming a 0.5 μm platelet contraction, the strain, ϵ, is then:

$$\epsilon = \frac{\Delta L}{L} = \frac{\sqrt{\delta^2 + L^2} - L}{20} = \frac{\sqrt{0.5^2 + 7.35^2} - 7.35}{7.35} = 0.0023$$

The associated angle is then:

$$\theta = \tan^{-1}\left(\frac{0.5}{7.35}\right) = 0.07$$

Due to symmetry in this system, and in consideration of static equilibrium, the force applied by the fibrin to the platelet is then:

$$Fsin\theta = E\ A\ \epsilon\ sin\theta = (14.5\ MPa)\left(\frac{\pi}{4}(284\ nm)^2\right)(0.0023)(\sin 0.07) = 0.15\ nN$$

When the platelet pulls the parallel to the fibrin strand, the extension is maximized. Assuming that the platelet is capable of pulling 0.5 μm, the associated strain is then:

$$\epsilon = \frac{\Delta L}{L} = \frac{0.5}{14.7} = 0.034$$

The force is then

$$F = E\ A\ \epsilon = (14.5\ MPa)\left(\frac{\pi}{4}(284\ nm)^2\right)(0.034) = 31\ nN$$

Also, if a platelet were pulling on unligated fibers in the developing clot (pre Factor XIII), then these values would be an order of magnitude lower. Hence, in examining these limiting cases and previously published values for platelet contraction, choosing PAA gels of stiffness between 5 and 100 kPa (Extended Data Figure 2d) will adequately cover the micromechanical stiffness environment that a platelet will experience within a typical clot.